Earth and Planetary Science Letters, 105 (1991) 266–278
Elsevier Science Publishers B.V., Amsterdam

[DT]

Tibetan tectonics from $^{40}Ar/^{39}Ar$ analysis of a single K-feldspar sample

Frank M. Richter [a], Oscar M. Lovera [b], T. Mark Harrison [c] and Peter Copeland [d]

[a] *Department of the Geophysical Sciences, University of Chicago, Chicago, IL 60637, USA*
[b] *Division of Geological and Planetary Sciences, California Institute of Technology, Pasadena, CA 91125, USA*
[c] *Department of Earth and Space Sciences and Institute of Geophysics and Planetary Physics, University of California, Los Angeles, CA 90024, USA*
[d] *Department of Geosciences, University of Houston, Houston, TX 77204-5503, USA*

Received May 20, 1990; revision accepted February 21, 1991

ABSTRACT

$^{40}Ar/^{39}Ar$ data on an alkali feldspar sample from the Quxu pluton, Gangdese batholith, southern Tibet, allow a detailed assessment of unroofing and uplift history between 35 and 18 Ma. The ^{39}Ar Arrhenius plot for this sample shows departures from a linear relationship between the effective diffusion parameter, $\log(D/r^2)$, and reciprocal temperature, which we interpret to be the result of a distribution of distinct diffusion-domain sizes. We use an alternative way of plotting the Arrhenius data that exhibits domain size versus cumulative % ^{39}Ar released during step heating. The $^{40}Ar/^{39}Ar$ age spectrum of the sample has features, such as local age plateaus, that are most easily explained in terms of the distinctive closure age of particular domains. The fact that the same distribution of diffusion-domain sizes explains both the Arrhenius data and the age spectrum is an indication that the diffusion properties operating in the laboratory are those of the sample while it was in its natural environment. Modelling of the age spectrum with a distribution of domain sizes results in the recovery of a continuous cooling-history segment rather than a single time–temperature datum. We demonstrate the robustness of the cooling-curve determination by showing the large misfits to the age spectrum that arise from relatively small changes in the cooling history. The best-fit cooling curve for the Quxu sample shows a decreasing rate of cooling in the time interval 35–18 Ma, followed by a very rapid cooling beginning at about 18 Ma. We have used a thermal model for the conductive cooling of an unroofing pluton to estimate the rate of unroofing required to explain the Quxu cooling curve, and find that in the 35–20 Ma time interval, the primary control of the thermal evolution is the conductive loss of magmatic heat with little or no unroofing (unroofing rates of approximately 0.05 mm/yr) followed by a brief period (< 5 Ma) of very rapid unroofing with rates of order 2 mm/yr.

1. Introduction

The uplift of the Himalaya and the Tibetan plateau is a classic example of mountain building by continent–continent collision; in this case the northward motion of India relative to Asia. The exceptionally high elevation of this area is a manifestation of this uplift, but of itself does not provide a measure of the timing or the total amount of vertical motion. The magnitude of this motion is certainly greater than the present topographic expression because of degradation by erosion. Additional information is needed to determine how much uplift and erosion has taken place, and how it was distributed both spatially and temporally.

This paper describes an application of $^{40}Ar/^{39}Ar$ thermochronometry [1] for quantifying the kinematics of geologic processes associated with mountain building, namely the rate at which minerals crystallized at depth are brought to the surface by erosion or tectonic unroofing. We use $^{40}Ar/^{39}Ar$ data from a single alkali feldspar sample separated from the Quxu pluton of the Gangdese batholith to determine both the cooling and unroofing history of the Quxu pluton. By unroofing, we mean the motion of the sample relative to the surface of the earth, regardless of how the surface may itself have moved relative to some other reference such as sea level.

The Gangdese (Transhimalayan) batholith (Fig. 1), which contains the Quxu pluton, lies just north

0012-821X/91/$03.50 © 1991 – Elsevier Science Publishers B.V.

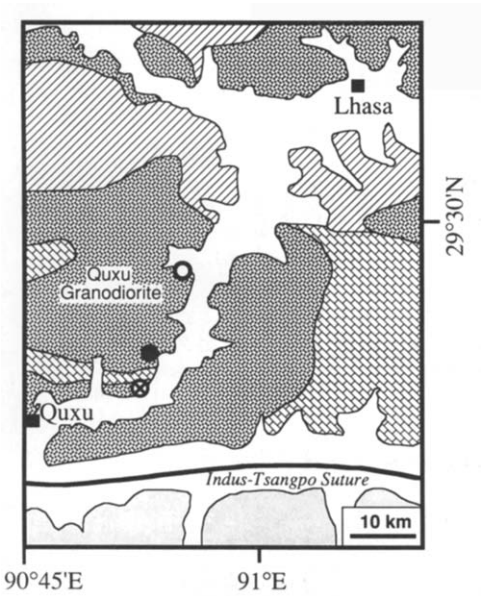

Fig. 1. Simplified geologic map of the study area, southern Tibet, after Kidd et al. [30]. Bold stippled area = granitoid rocks of the Gangdese batholith; inclined lines = Paleozoic and Mesozoic sedimentary rocks; inclined brick pattern = carbonates, amphibolites, and sandstones (mostly Mesozoic) metamorphosed by contact with plutons of the Gangdese batholith; lightly shaded pattern = Triassic silt and mud turbidites; unpatterned areas = Quaternary; filled circle = sample site of PC-88-32 (this study); open circle = location of samples studied by Copeland et al. [20]; circle with X = location of sample P-5-1-88.

of the Indus–Tsangpo suture zone marking the geologic boundary between India and Asia. It is a large (about 50 km across by more than 2600 km along strike), I-type [2], composite batholith with an average composition of granodiorite [3]; crystallization ages range from 110 to 40 Ma [4,5]. The collision between India and Asia is generally thought to have begun between 50 Ma [6–8] and 40 Ma [9], with some estimates as old as 65 Ma [10]. Before the collision, the Gangdese belt was an Andean-type convergent margin at the southern edge of Asia. Following the collision of India with Asia, a further convergence of at least 2000 km has taken place [11,12] accommodated by a combination of north–south crustal thickening and motion along large displacement faults [9,13–17]. The history of, unroofing that we document for the Quxu pluton is almost certainly a result (and a monitor) of crustal thickening and uplift in the area.

We focus on the results derived from a single sample to dramatize the wealth of thermochronometric information that K-feldspars contain. In its traditional application, the $^{40}Ar/^{39}Ar$ method (see [18] for a detailed exposition of the method) is used to date the time when ^{40}Ar, a product of ^{40}K decay, began to be retained by a mineral. The age so determined will often be considerably younger than the crystallization age of the mineral because at high temperatures, greater than about 300°C for alkali feldspars, ^{40}Ar will be lost by thermally activated diffusion as fast as it is being produced by decay, and thus ^{40}Ar will not accumulate to record the passage of time. Only after the temperature falls below the closure temperature [19], will ^{40}Ar begin to be retained. Thus, the K-Ar age of a mineral that has cooled slowly reflects the time before present that the rock reached the closure temperature. By this approach one determines a single age and a single closure temperature for each sample analyzed.

Our recent work [1,20,21] on the $^{40}Ar/^{39}Ar$ age spectra (age as a function of Ar released during step heating) and Ar diffusion properties of K-feldspars provides evidence that these minerals can be described by a distribution of discrete domains with different Ar diffusion properties, particularly the effective frequency factor for thermally activated diffusion. As a result, feldspars will often record not a single closure temperature but an entire segment of the cooling history of the sample for periods that can be as long as several tens of millions of years. This being true of the K-feldspar separate from the Quxu pluton, we were able to determine a thermal history that reflects the cooling of the intrusion over the period 41–20 Ma, with little or no unroofing, followed by a very rapid cooling that we interpret as being due to high rates of unroofing of the order of several mm/yr.

The unroofing rates as a function of time inferred from the single feldspar sample discussed in this paper are very similar to those determined earlier by Copeland et al. [22] for a nearby part of the Quxu pluton using a different approach involving five samples collected over a range of elevations and dated using $^{40}Ar/^{39}Ar$ and fission track methods. The agreement between these two different approaches gives an important measure of confidence in both. The demonstration that

TABLE 1

PC-88-32 K-feldspar

Temp. (°C)	$^{40}Ar/^{39}Ar$	$^{37}Ar/^{39}Ar$	$^{36}Ar/^{39}Ar$ (10^{-3})	^{39}Ar (10^{-13} mol)	% ^{39}Ar released	$^{40}Ar^*$ (%)	$^{40}Ar^*/^{39}Ar_K$	Age ± 1 s.d. (Ma)	Time (min)	10,000/T (K)	log(D/r^2) (s^{-1})	log(r/r_0)
450	472.700	0.0000	1394.0000	0.131	0.106	12.8	60.780	305.0 ± 32.0	15	13.83	−9.009	−0.087
510	37.170	0.3214	63.5800	0.181	0.252	48.7	18.390	98.0 ± 8.0	18	12.77	−8.420	0.143
570	8.851	0.0749	1.5910	0.998	1.060	93.5	8.374	45.3 ± 0.7	22	11.86	−7.201	−0.017
630	5.399	0.0482	2.3830	1.710	2.440	85.9	4.687	25.5 ± 0.9	17	11.07	−6.428	−0.014
700	4.271	0.0233	0.7991	4.340	5.950	93.7	4.025	21.9 ± 0.6	15	10.28	−5.590	−0.043
760	3.883	0.0158	0.0331	5.700	10.500	99.0	3.863	21.0 ± 0.2	13	9.68	−5.116	0.017
800	3.687	0.0004	0.5196	5.610	15.100	95.1	3.523	19.2 ± 0.4	16	9.32	−5.022	0.148
800	3.698	0.0180	0.5848	4.450	18.700	94.5	3.515	19.2 ± 0.4	22	9.32	−5.141	0.207
725	3.790	0.0164	0.5048	11.900	28.300	95.6	3.631	19.8 ± 0.2	874	10.02	−6.171	0.377
820	3.713	0.0654	1.5850	0.746	28.900	84.1	3.237	17.6 ± 0.8	37	9.15	−5.916	0.679
870	3.934	0.0594	0.2967	0.659	29.400	93.9	3.838	20.9 ± 0.3	16	8.75	−5.595	0.716
920	4.062	0.0361	0.4792	2.020	31.000	95.1	3.911	21.3 ± 1.1	15	8.38	−5.066	0.634
970	4.181	0.0403	0.2731	3.280	33.700	97.1	4.092	22.3 ± 0.4	17	8.05	−4.789	0.658
1010	4.563	0.0156	0.7222	4.110	37.000	94.6	4.340	23.6 ± 0.2	17	7.79	−4.742	0.764
1040	5.000	0.0130	0.4083	4.040	40.300	96.9	4.869	26.5 ± 0.2	12	7.62	−4.560	0.756
1060	5.348	0.0069	0.2073	7.410	46.200	98.4	5.276	28.7 ± 0.2	24	7.50	−4.549	0.811
1080	5.350	0.0058	0.8412	4.680	50.000	94.8	5.091	27.7 ± 0.2	14	7.39	−4.468	0.824
1100	5.468	0.0098	0.5698	5.970	54.800	96.4	5.290	28.8 ± 0.2	16	7.28	−4.382	0.835
1120	5.544	0.0160	0.6053	3.440	57.600	96.1	5.355	29.1 ± 0.4	13	7.18	−4.502	0.945
1120	5.575	0.0534	0.7300	3.240	60.200	95.4	5.351	29.1 ± 1.2	20	7.18	−4.666	1.027
1120	5.575	0.0308	0.8259	2.730	62.400	94.8	5.322	28.9 ± 0.6	20	7.18	−4.715	1.052
1120	5.692	0.0097	0.5130	4.560	66.100	96.8	5.530	30.0 ± 0.2	43	7.18	−4.789	1.088
1120	5.834	0.0143	0.1076	5.280	70.400	99.0	5.792	31.5 ± 0.2	77	7.18	−4.927	1.157
1120	6.023	0.0003	0.1790	6.500	75.600	98.7	5.960	32.4 ± 0.2	114	7.18	−4.936	
1120	6.089	0.0172	0.5821	15.500	88.100	96.9	5.907	32.1 ± 0.1	860	7.18	−5.247	
1170	6.284	0.0084	0.4683	3.540	91.000	97.2	6.135	33.3 ± 0.2	40	6.93	−4.330	
1500	6.159	0.0713	0.6590	11.100	100.000	96.6	5.957	32.2 ± 0.2				

$J = 0.003037$, wt. = 113.18 mg, $E = 45.2$ kcal/mol, $D_0/r_0^2 = 3.03 \times 10^4$ s^{-1}.

equally good results can now be obtained by analysis of a single sample suggests that future regional studies for the spatial and temporal distribution of unroofing can be carried out with a relatively small number of samples.

2. Experimental results

A high-purity K-feldspar separate (K_2O concentration 13.5%) was obtained from a granodiorite sample (PC-88-32) of the Quxu pluton collected at an elevation of 4560 meters about halfway between Lhasa and Quxu (Fig. 1). Sample preparation, irradiation and $^{40}Ar/^{39}Ar$ isotopic analysis followed the procedures of Harrison and Fitz Gerald [23] and Harrison et al. [21]. The $^{40}Ar/^{39}Ar$ data for this sample are given in Table 1.

Figure 2 is an Arrhenius plot for the Quxu sample showing $\log(D/r^2)$ versus reciprocal temperature. This plot is constructed by interpreting the amount of ^{39}Ar released during step heating (the temperature and duration of each step is shown in the inset) in terms of a diffusivity D for a slab of thickness r. If the sample contained a uniform distribution of ^{39}Ar prior to step heating, and only one characteristic diffusion domain size, and the thermally activated diffusion of argon followed a simple Arrhenius law, all the data shown in this plot would all fall on a single straight line. Clearly they do not and at least one of the above requirements is not met. Recall that ^{39}Ar is produced from ^{39}K by fast-neutron irradiation and thus the reasonable expectation is that it will be just as uniformly distributed as potassium. The more likely explanation of the departures from a straight line in the Arrhenius plot is that this sample is composed of a distribution of diffusion domains of different size. The departures from linearity in the Arrhenius plot are then the result of the smaller domains releasing their argon first (the linear data trend at low temperature is for this first-released gas), followed by argon from larger domains that will plot at lower values of $\log(D/r^2)$ because of their larger r. Although the activation energies for the larger domains may be slightly higher than that given by r_0 [21], it is unlikely to affect the unroofing history calculated assuming constant activation energies.

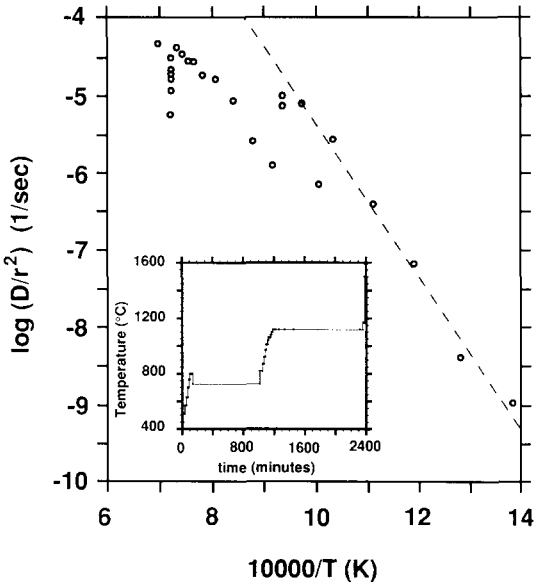

Fig. 2. Arrhenius plot of $\log(D/r^2)$ versus reciprocal absolute temperature for the sample PC-88-32. See Harrison and McDougall [31] for a description of how diffusion coefficients are calculated from ^{39}Ar released during step heating. The diffusion domain geometry assumed is slabs, but this is not a key assumption in that experience with this and other samples has shown us that as long as we use the same geometry for both data analysis and modelling, the cooling curve determined will be the same regardless of what specific geometry (slab, cylinder, or sphere) is used. The inset shows the temperature steps used to extract ^{39}Ar. All but the last two steps are well below the melting temperature of the sample, which is important for resolving the diffusion properties of the largest domains in the sample. The dashed line corresponds to an activation energy E of 45.2 kcal/mol and an effective frequency factor, D_0/r_0^2, of 30,300 s^{-1}.

The $^{40}Ar/^{39}Ar$ age spectrum of the Quxu sample (Fig. 3a) gives further evidence of different diffusion domains. A sample made up of diffusion domains of a single characteristic size should have an age spectrum that increases smoothly with cumulative % ^{39}Ar released (see [1] for calculated age spectra of single and multi-domain samples), while the age spectrum of the Quxu sample shows several local plateaus at 10–30, 40–60 and 70–100% ^{39}Ar released. Such local plateaus will be produced by the distinct closure temperature and age associated with each domain size fraction. The decreasing ages seen for the first 10% of argon released are a common feature of many feldspar age spectra. These anomalous ages are generally attributed to excess argon taken up at grain

margins at geologically low temperatures (see discussion of excess argon in [18]), and are ignored when assessing cooling histories. In the modelling that follows we will ignore this excess argon. We feel particularly justified in this case as an age spectrum from a nearby (Fig. 1) K-feldspar sample (P-5-1-88) is unaffected by excess argon and yields ages early in release of 19–20 Ma (Fig. 4).

Up to this point, we have argued that both the Arrhenius plot and the age spectrum have features that will arise if a sample is made up of diffusion domains of different size. However, the two plots cannot be directly compared because in one case the property affected by domain size is plotted against reciprocal temperature while in the other it is plotted against cumulative % ^{39}Ar. What is needed is a different graph that exhibits the domain-size information of the Arrhenius plot as a function of cumulative % ^{39}Ar. We proceed as follows. The straight dashed line drawn in Fig. 2 can be represented by an Arrhenius relation of the form:

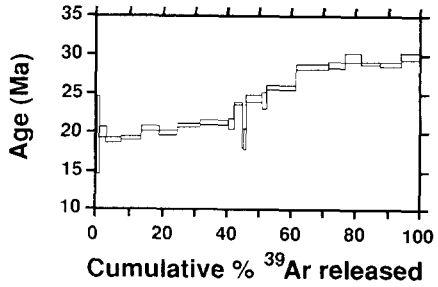

Fig. 4. ^{40}Ar/^{39}Ar age spectrum for K-feldspar sample P-5-1-88. This sample, unaffected by excess argon, yields ages early in gas release that support our view that the Quxu pluton experienced very rapid cooling beginning at about 20 Ma.

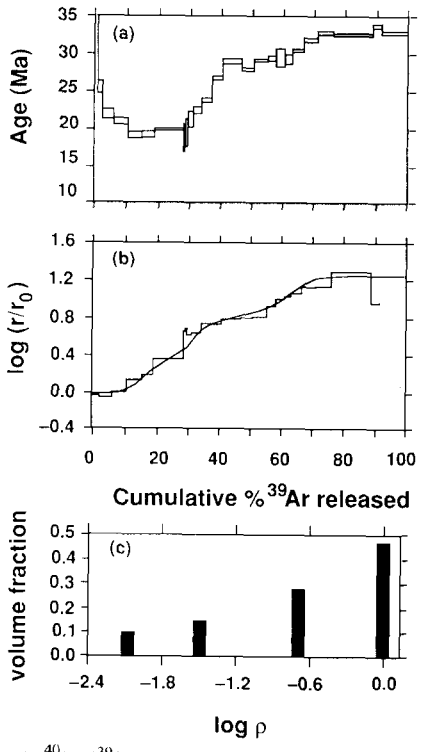

Fig. 3. (a) ^{40}Ar/^{39}Ar age spectrum for K-feldspar sample PC-88-32. (b) $\log(r/r_0)$ versus cumulative % ^{39}Ar calculated for the distribution of domains (shown in 3c) compared to the actual data from the Quxu sample. The last two fractions of ^{39}Ar are ignored because they were extracted at such high temperature that the sample is beginning to melt and therefore the diffusion properties determined from these steps are not representative of the sample when in its natural environment. (c) size (ρ) and volume fraction (ϕ) of domains used in modelling. The relative size (and volume fraction), of each domain, from largest to smallest are: 1.00 (10%), 0.320 (15%), 0.056 (30%), and 0.01 (45%), respectively.

$$D(T)/r_0^2 = \left(D_0/r_0^2\right) e^{-E/RT} \tag{1}$$

where $D(T)$ is the diffusivity of argon at temperature T, r_0 is a reference domain size, D_0 is the intrinsic frequency factor, E is the activation energy, and R is the gas constant. The vertical distance on the Arrhenius plot between each data point and this line can be written as:

$$\log\left(D(T)/r^2\right) - \log\left(D(T)/r_0^2\right) = 2\log(r/r_0) \tag{2}$$

thus, with each data point we can associate an apparent domain size r, relative to the reference domain size r_0. In an earlier paper [1] we showed that:

$$r_0 = \left\{\sum_{j=1}^{s} \left(\phi_j/\rho_j\right)\right\}^{-1} \tag{3}$$

and is in general obtained from the best-fitting straight line through the linear low-temperature portion of the Arrhenius plot (e.g., Fig. 2). The summation is taken over the s distinct domains present in the sample, each of size ρ_j, each representing a volume fraction ϕ_j of the total sample.

We can also associate a cumulative % ^{39}Ar released with each data point in the Arrhenius plot, and thus create a graph of $\log(r/r_0)$ versus cumulative % ^{39}Ar as shown in Fig. 3b. If the

sample was composed of a single dominant diffusion domain size, this figure would show all data lying along $\log(r/r_0) = 0$. What we actually find is that only the first 10% of the released argon lies near $\log(r/r_0) = 0$ (we don't disregard the first 10% of ^{39}Ar released since the problem of excess argon mentioned earlier involves only ^{40}Ar). Subsequent $\log(r/r_0)$ values rise to as high as 1.2; we associate this increase with argon released from larger domains. We can now see more clearly that both the age spectrum and the $\log(r/r_0)$ plot suggest the existence of more than one diffusion domain size in the Quxu sample. The plateaus in the age spectrum are slightly shifted to higher cumulative % ^{39}Ar than those one might pick in the $\log(r/r_0)$ plot, but as we will show later by model calculations, this is exactly what one should expect.

Experience with other feldspar samples subject to a variety of different heating schedules has taught us that one has to be quite careful with the temperature steps used to extract argon for a useful $\log(r/r_0)$ to be produced [20,21]. In particular, one must avoid melting the sample, because the $\log(r/r_0)$ of argon extracted at or above the incongruent melting temperature (1150°C) will have low values. The data shown in Fig. 3 were produced by extraction at temperatures less than or equal to 1120°C for all but the last 12% of argon released. The low value of $\log(r/r_0)$ for 88–91% cumulative % ^{39}Ar is due to an extraction temperature of 1170°C. The final 9% of argon was extracted at 1500°C, well above the melting temperature, and thus also gives no relevant information regarding the diffusion properties that the sample had while in its natural environment.

3. Modelling

We quantify the thermochronometric information contained in the Quxu sample by first finding through repeated forward modelling a distribution of domain sizes that can account for the data shown in the Arrhenius plot and the shape of the $\log(r/r_0)$ plot. Once the Arrhenius parameters and the size and proportion of domains have been assessed we can proceed to calculate age spectra for different cooling histories until we find one that produces a good fit to the observed age spectrum. The governing equations and methods of solution for calculating Arrhenius plots and age spectra for multi-domain samples are discussed in detail in Lovera et al. [1].

Since our interest is not so much cooling *per se* but what it can tell us about unroofing, we will also have to model the thermal environment of the sample as it changes in response to thermal diffusion during unroofing. It is this step that will allow us to infer unroofing rates from a cooling curve.

Figure 3b shows the calculated $\log(r/r_0)$ versus cumulative % ^{39}Ar for a sample made up of four distinct diffusion domains and compares it to the experimental data from sample PC-88-32. The domain distribution which best matches the Arrhenius data contains four distinct domains with the largest size about 100 times greater than the smallest. The degree of fit to the actual data could have been further refined, but our experience with this and other samples has shown that introducing a greater number of distinct domains does not have a significant effect on the calculated age spectrum and cooling curve of the sample [20].

Figure 5 shows calculated age spectra for a sample having the domain distribution of Fig. 3c and the cooling histories shown in Fig. 5a. Aside from the ages of the first 10% ^{39}Ar released (which we earlier argued could be ignored), the cooling history labeled "b" (bold line) reproduces the measured age spectrum rather well, particularly the local age plateaus associated with the different size diffusion domains (Fig. 5b). This fit between calculated and measured age spectrum is very sensitive to the details of the cooling curve, which leads us to believe that we have in fact resolved, within rather narrow bounds, the actual cooling history of the sample. The sensitivity of the age spectrum to particular details of the cooling curve is illustrated by Fig. 5c–f. In Fig. 5c we show the age spectrum calculated assuming that the rate of cooling around 30 Ma continues unchanged until 15 Ma (dot-dashed line, Fig. 5a). For this uniform cooling rate, we fail to reproduce the abrupt decrease in age between 30 and 40% ^{39}Ar released because the second smallest domain is closing to argon diffusion much too soon. At the other extreme we can consider what happens if the more rapid cooling rate of the 18–15 Ma period were typical of the entire cooling history (dashed line, Fig. 5a). In this case, all the domains close at

much the same time and far too flat a spectrum results (Fig. 5d). Fig. 5e shows the effect on the age spectrum of simply not having a period of rapid cooling prior to 15 Ma (thin solid line, Fig. 5a), while Fig. 5f shows the effect of shifting the onset of rapid cooling to 22 Ma (dotted line, Fig. 5a). In both cases we find age spectra that are clearly poor fits to the measured data. The sensitivity of the age spectra of multi-domain samples to details of the thermal history is highly constrained (on the order of $\pm 25°C$, ± 1 Ma) by our model fit to the observed age spectrum of the Quxu sample.

A reasonable question to ask at this point is what is the nature of the diffusion domains? Before addressing this, we point out the importance of not confusing our lack of definitive understanding of this query with our ability to reconstruct geological thermal histories. In the extreme view, the multi-domain model is simply a metaphor for whatever the responsible diffusion process(es) are. Provided that the diffusion behavior observed in the laboratory reflects the same processes operating in the natural environment, thermal history results are insensitive to the formulation of the diffusion model. In other words, the model need

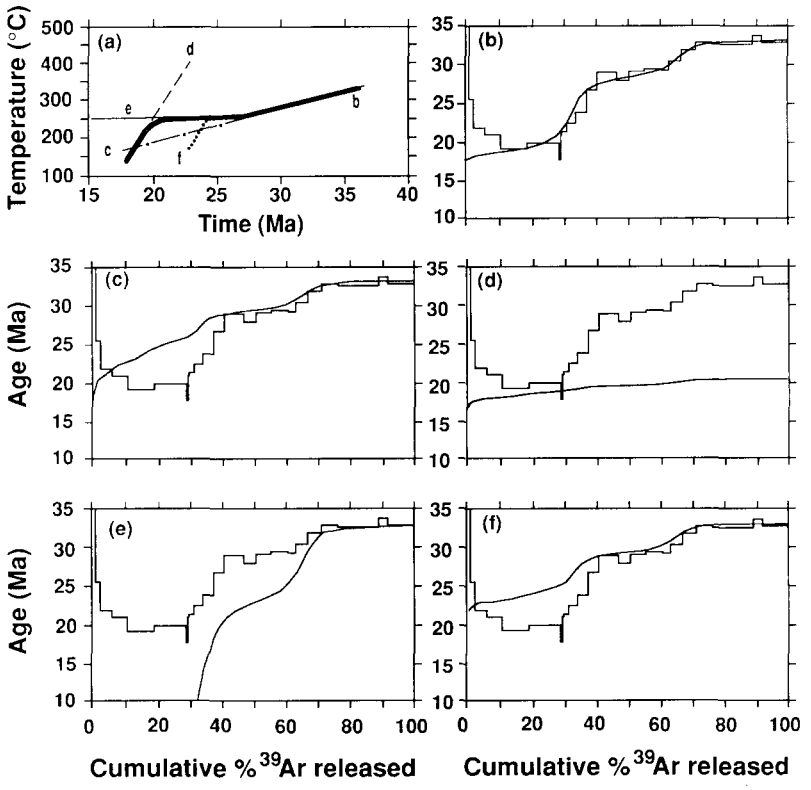

Fig. 5. (a) Cooling histories used in age spectrum modelling of sample PC-88-32; In (b) through (f), the $^{40}Ar/^{39}Ar$ age spectra calculated for each cooling history given in (a) are shown using the distribution of domains shown in Fig. 3c (assuming that they all have the same activation energy of 45.2 kcal/mol). (b) This synthetic spectrum, calculated using the thermal history shown in (a) by the bold solid line, is a good fit to the experimental data except for the first 10% of argon released, which is obviously affected by extraneous argon. (c) This figure shows the misfit between the calculated age spectrum and experimental data if we assume a uniform rate of cooling equal to that used in (b) from 35 to 27 Ma [dot-dashed curve in (a)]. For this uniform cooling rate, the second smallest domain closes much too early, resulting in an age spectrum that is clearly unacceptable. (d) This shows the calculated age spectrum assuming a constant rate of cooling equal to that used in (b) at about 17 Ma [dashed line in (a)]. The calculated age spectrum is now far too flat because at this rapid cooling rate all domains close at much the same time; (e) This shows the effect of removing the period of rapid cooling used in (b) [thin solid line in (a)] Only the very largest domain closes at the appropriate time, all others close much too late; (f) This shows the effect of shifting the onset of rapid cooling from around 19 to 23 Ma [dotted line in (a)], and we find that the second smallest domain closes much too early.

not reflect the actual atomistic and/or mineralogic features in order to be an effective conduit for the thermal history information. Nonetheless, several lines of evidence are emerging which suggest that microstructural features observable by TEM (e.g., exsolution boundaries) may define Ar diffusion boundaries in silicates (see [21] and references therein).

The next step is to relate the cooling curve of the Quxu sample to the processes that controlled its thermal history. The sample comes from a pluton emplaced at a temperature of about 800–850°C at approximately 42 Ma [4], therefore one process we must certainly consider is the conductive cooling of the pluton itself. The second process involved is the motion of the sample towards the surface of the earth. Al-geobarometry (using the calibration of Johnson and Rutherford [25]) on a nearby hornblende from the same pluton, and very nearly the same elevation as our sample, suggests that the Quxu rocks presently at the surface crystallized at a depth of 10 km. Given our incomplete understanding of the physical conditions during crystallization (e.g., f_{H_2O}) we associate an uncertainty of 2 km to this value. This gives an average unroofing rate for the area of about 0.3 mm/yr. Inspection of the bold cooling curve shown in Fig. 5a suggests that we are seeing the general cooling of the pluton with little or no unroofing up to about 20 Ma followed by a brief interval of rapid uplift and unroofing. To confirm and quantify this, one needs to explicitly model the thermal evolution of a pluton that is cooling while being uplifted and eroded at a variable rate.

The thermal model we use for the Quxu pluton is shown in Fig. 6. The general approach follows that of Harrison and Clarke [26]. We assume that at 42 Ma the presently exposed level of the Quxu and other nearby plutons were emplaced at a depth of 10 km in a belt 40 km in N–S extent and about 100 km long in an E–W direction. Their intrusion temperature is taken to be 950°C and they are emplaced into rocks with a geothermal gradient $T_i(z)$. The intrusion temperature of 950°C represents an actual emplacement temperature of 850°C with an additional 100°C to account for the latent heat of crystallization. Given the assumed aspect ratio of the belt of plutons, we can consider a two-dimensional model of a N–S section as shown in Fig. 6. Sample PC-88-32 is assumed to have come from an initial depth of 11 km along the axis of the intrusive belt. The entire system moves upwards relative to the surface at a rate $W(t)$, which we can vary with time. Our goal is to find $W(t)$ such that the model sample has a calculated cooling curve in good agreement with that given by the $^{40}Ar/^{39}Ar$ method.

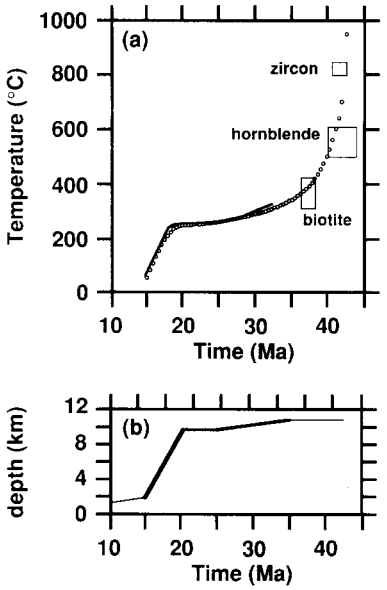

Fig. 6. The top panel shows the geometry and boundary conditions for the thermal model of the cooling and uplift of the Quxu pluton. The stippled area represents the intrusion of the Quxu pluton at 41 Ma, which reaches to within 10 km of the surface. The large black dot shows the initial position of the model Quxu sample at 11 km depth. The intrusion temperature is taken to be 950°C (850°C + an additional 100°C to represent heat of crystallization) at those depths where this temperature is greater than that of the regional geotherm $T_i(z)$, shown in the lower panel. This geotherm is a steady state solution to the heat conduction equation with heat sources $Q(z)$ when the vertical velocity relative to the surface $W(t)$ is zero. The boundary conditions and our choices for $Q(z)$ and $W(t)$ are discussed in the text.

The least well-constrained aspect of our modeling of the cooling history of the Quxu pluton involves specifying the regional thermal structure $T_i(z)$ that would exist in the absence of intrusion and unroofing. We will return to this point later to suggest how particular sampling strategies and additional $^{40}Ar/^{39}Ar$ data can be used to better constrain $T_i(z)$, but for the moment we will proceed by assuming that $T_i(z)$ is like the average continental geotherm of Sclater et al. [27].

The thermal evolution equation we solve is:

$$\rho c_p \{ \partial T/\partial t + W(t)\ \partial T/\partial z \} = k \nabla^2 T + Q(z) \tag{4}$$

where ρ is density ($= 3 \times 10^3$ kg/m^3), c_p is the specific heat ($= 10^3$ J/kg°C), T is temperature in °C, t is time in seconds, $W(t)$ is vertical velocity in m/s, k is thermal conductivity ($= 3$ W/m°C), and $Q(z)$ is radiogenic heat production as a function of depth in W/m^3. The boundary conditions on temperature are $T = 0$°C at the surface $z = 0$, a mantle heat flux F_R (25 mW/m^2) at a depth $z = 100$ km, and $\partial T/\partial x = 0$ for all z at $x = 0$ and $x = 200$ km. The condition at $x = 0$ implies reflection symmetry, while the condition at $x = 200$ is sufficiently far from the intrusion so as to not affect the solution over the period of time it is calculated. We choose $Q(z)$ to be an exponentially decaying function of depth with a length scale δ of 10 km [27] and with a magnitude that in the steady state would result in a surface heat flux $F = 100$ mW/m^2, typical of many continental areas [24]. Thus:

$$Q(z) = \{ (F - F_R)/\delta \}\ e^{-(z/\delta)} \tag{5}$$

For the initial temperature distribution away from the intrusion [$T_i(z)$] we use the steady state solution of equation (4) given by:

$$T_i(z) = \{ F_R z + (F - F_R)\delta(1 - e^{-(z/\delta)}) \}/k \tag{6}$$

while for the intrusion itself we use an initial temperature of 950°C from 10 km to the depth where $T_i(z)$ equals 950°C. Figure 6 includes a panel showing the geotherm $T_i(z)$.

The thermal evolution equation is solved numerically by standard techniques [28] for different choices of $W(t)$. Keeping in mind that the sample is also moving towards the surface at a rate $W(t)$, we determine the temperature of the sample as a function of time, and change $W(t)$ until we find reasonably good agreement between the calculated sample cooling curve and that of the Quxu sample. Figure 7a compares such a calculated cooling curve to that found earlier from the age spectrum of the Quxu sample. Also shown are temperature–time estimates derived from the age of zircons [4], nearby hornblendes [22], and a biotite from PC-88-32 [24] together with closure and crystallization temperatures. Figure 7b shows

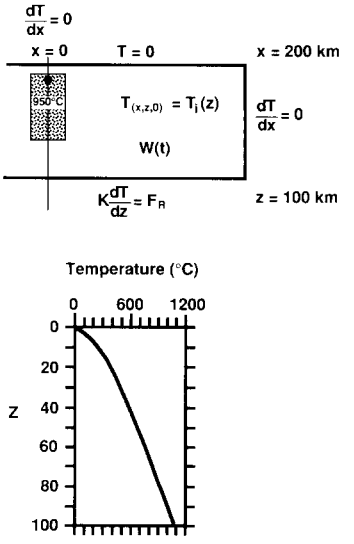

Fig. 7. (a) Cooling history of the Quxu pluton. The open circles follow the cooling history for a model sample calculated using our thermal model for an unroofing pluton (Fig. 6) with $W(t)$ such that the sample's depth changes as shown by the heavy line segments in (b). This thermal history is in good agreement with the cooling curve determined earlier from the age spectrum of the feldspar separate from PC-88-32 (curve *b* in Fig. 5a), shown by the heavy line segments. Additional information regarding the cooling of the Quxu pluton is obtained from concordant U-Pb ages [4] (41.5 ± 0.5), which we associate with an effective intrusion temperature of 900–950°C (see text), the average age of Quxu pluton hornblendes [22] which have a closure temperature of 550°C ± 50°C., and the age and closure temperature (370°C ± 50°C) of a biotite also separated from sample PC-88-32 [24]. (b) The model depth as a function of time for sample PC-88-32. The heavier line segments are constrained by our fit of the age spectrum of the K-feldspar from PC-88-32, while the thinner line segment represents a uniform rate of unroofing that would bring the sample from a depth of 2 km to its present location on the surface.

the depth of the model sample as a function of time. We could have refined the fit of the calculated cooling curve to that of the Quxu sample by further changing the vertical velocity as a function of time, but given the idealized thermal model used there is little point in doing so. We prefer to show that a very simple history of unroofing already gives a good approximation to the cooling curve of the Quxu sample determined from the $^{40}Ar/^{39}Ar$ data.

The results of the thermal modelling suggest that the Quxu pluton was unroofing at a relatively slow rate — between zero and 0.1 mm/yr — from 42 to 20 Ma. During this stage the cooling

curve is dominated by the conductive loss of the original high temperature of intrusion. Starting at 20 Ma, there was a brief period of very rapid unroofing that moved the analyzed sample towards the surface at a rate on the order of 2 mm/yr. Since this would place the sample at about 2 km depth at 15 Ma, there must have followed a period of slow unroofing with rates not much greater than 0.1 mm/yr bringing the sample to the present surface of the earth. Note that there is a time lag of about 1 million years between the onset of rapid unroofing and its effect being felt thermally by the sample. This is due to the isotherms being advected during rapid upward motion of the crust.

4. Summary and discussion

Both the $^{40}Ar/^{39}Ar$ age spectrum (Fig. 3a) and ^{39}Ar Arrhenius plot (Fig. 2) of a K-feldspar sample from the Quxu pluton show evidence for a distribution of argon diffusion domains of different size. In an effort to bring out more clearly the implications of the data points not all falling on a straight line in the Arrhenius plot, we plotted the data in terms of $\log(r/r_0)$ versus cumulative % ^{39}Ar (Fig. 3b), where r is a measure of domain size relative to the effective domain size r_0 for the first few % of ^{39}Ar released. This manner of plotting Arrhenius data has the added benefit of allowing one to estimate the proportion of argon contained in domains of a particular size.

We then used numerical calculations for the release of ^{39}Ar from a multi-domain sample to determine more quantitatively the relative size and argon content of the different domains of the Quxu sample (Fig. 3c). Given this distribution of domains, we again used numerical calculations to find a thermal history for the sample that produces a good fit to the measured age spectrum (Fig. 5). An important point is that in modelling the Arrhenius plot (or equivalently the $\log(r/r_0)$ plot) and the age spectrum of the Quxu sample we had to represent the sample as being made up of a distribution of different argon diffusion domains. Indeed, the same distribution of domains can be used to model both the Arrhenius data and the age spectrum. The importance of this is that the Arrhenius data are the result of processes that took place in the laboratory (diffusion of ^{39}Ar during step heating) while the age spectrum is the reflection of ^{40}Ar closure during slow cooling in nature. That these very different processes end up reflecting the same diffusion domain distribution is the best evidence that the diffusion parameters determined in the laboratory are in fact relevant to the retention of argon by the sample on geological time scales while in its natural environment.

On the basis of additional calculations that test the sensitivity of age spectra to particular details of a sample's cooling history (Fig. 5), we concluded that the cooling curve of the Quxu sample is resolved to about $\pm 25°C$ in temperature and ± 1 Ma in time. The best-fit cooling curve for the Quxu sample shows a slow cooling rate from about 35 to 26 Ma, negligible cooling from 26 to 19 Ma, followed by much more rapid cooling in the time interval 19 to perhaps 15 Ma. Using a numerical model (Fig. 6) for the thermal evolution of a sample contained in a pluton emplaced at 42 Ma and subject to unroofing we demonstrate that the cooling curve of the Quxu sample can be accounted for by the cooling of the intrusion with relatively little unroofing in the 42–20 Ma time interval followed by very rapid unroofing from 20 to about 15 Ma (Fig. 7).

The thermal modelling that we have used to relate cooling to unroofing has several potential limitations. One of these is that we are assuming that the thermal structure of the area evolves by conduction and vertical motion of the region as a whole. It is possible that in some stages of the region's evolution, particularly during those involving rapid uplift and erosion, hydrothermal fluids might have played a role in removing heat. If this were the case, we could easily misinterpret the rapid cooling due to fluid advection as being the result of rapid unroofing. However, the published values of δD and $\delta^{18}O$ of biotites and hornblendes from gabbroic and granodioritic phases of the Quxu pluton [29] suggest that exchange with hydrothermal fluids has not occurred, and thus a conductive model for cooling is reasonable.

We have already mentioned another limitation arising from the lack of independent data with which to constrain the geothermal gradient in the vicinity of the analyzed sample. The effect of using a different geothermal gradient would be to

shift the sample's estimated depth as a function of time in proportion to the difference between the geothermal gradients used. Thus a key step for using cooling curves to make accurate statements about unroofing is to obtain additional data with which to constrain the geothermal gradients *at the time the samples were going through closure*. Since what is required is information about a thermal regime in the past, the most obvious way to proceed is again by $^{40}Ar/^{39}Ar$ measurements, but now on samples obtained from different elevations. We have calculated age spectra for model samples separated vertically by two kilometers assuming that each of these samples has the same argon diffusion properties as the sample PC-88-32. We conclude that such results, when inverted for cooling curves, would give useful information about the change of temperature gradient with time. Knowledge of the actual mechanisms of cooling could then be assessed. If, for example, the cause of cooling was hydrothermal circulation rather than unroofing, one would expect to see the evidence for this in a marked reduction of the vertical temperature gradient seen by those samples that have entered the hydrothermal zone.

A fair question to ask at this point is whether there exists any independent confirmation of the unroofing rates we have determined using a single feldspar sample from the Quxu pluton. The only other study of unroofing rates in this part of Tibet with comparable resolution to the results presented here is by Copeland et al. [22] using samples collected about 10 km further north, but still in the Quxu pluton (Fig. 1). The Copeland et al. [22] study used single-domain argon closure temperatures from hornblendes, biotites, and alkali feldspars sampled at different elevations, as well as an apatite fission-track age, to find the unroofing/uplift history of the Quxu pluton. Unfortunately, the laboratory heating schedule used for the feldspars by Copeland et al. [22] reached the temperature of incongruent melting at about 30 to 50% ^{39}Ar released and therefore meaningful diffusion data for the larger domains was not obtained; we will have to remeasure these samples before using them to constrain the geothermal gradient during closure by the approach mentioned above. The important point is that while the previous approach was different from the one used here, the results are remarkably similar. They suggest unroofing rates of 0.07 mm/yr for the period ending at 20 Ma, which falls within the range 0–0.1 mm/yr that we find. Copeland et al. [22] found that the rate of unroofing increased dramatically at 20 Ma to values of several mm/yr, which again is what we have found. We also agree that this period of rapid unroofing must have been short lived and followed by rates significantly less than 1 mm/yr.

The approach used by Copeland et al. [22] is less sensitive to the choice of geothermal gradient than ours because in their case the unroofing rates are based for the most part on the time that samples from different elevations went through closure. The only assumption then required is that the geothermal gradients have not changed significantly over the time that all their samples closed. The geothermal gradient that we used to translate cooling into unroofing was not selected to produce good agreement with the Copeland et al. [22] study; it is simply a typical continental geotherm. The agreement between the two studies is therefore a fair measure of both the methods used and the associated assumptions.

From the point of view of establishing the kinematic evolution of collision zones and constraining geodynamic models, the most relevant information is that relating to vertical motions relative to a geopotential surface such as sea level. What we have been able to determine for the Quxu pluton is an unroofing or denudation rate, which strictly speaking is vertical motion relative to the surface that might itself have moved relative to sea level. If we take the extreme position that the surface of the earth could have been anywhere between sea level and five kilometers above sea level during the period of rapid unroofing that we have documented, the actual vertical motion relative to sea level could have been as much as 50% larger than the 2 mm/yr unroofing rate shown in Fig. 7b. Clearly there was a distinct and short lived period of very rapid vertical motion relative to sea level beginning at 20 Ma. The real vertical velocity is likely to be close to the unroofing rate because appeals to such things as sudden erosion of a pre-existing high standing terrain due to climate change or the first appearance of external drainage are difficult to reconcile with many geological and geomorphological observations (summarized by Copeland et al. [22]). Furthermore,

one should keep in mind that crustal unroofing of the order of 8 km will drive very significant vertical velocities as a result of isostacy. Thus, we feel there is now good evidence of very high rates of uplift for the Quxu pluton during the early Miocene. The more important issue is the degree to which this local uplift is representative of uplift over the rest of southern Tibet and the Himalaya. In this connection, we feel that the methods described in this paper using a single feldspar sample combined with vertically arrayed samples, as suggested, should provide an efficient and effective approach for regional studies of unroofing and uplift.

Acknowledgements

Sample PC-88-32 is part of a collection made with help from W.S.F. Kidd, State University of New York at Albany. The age spectrum for sample P-5-1-88 was measured by Pan Yun and we thank him for allowing us to include it here. F.M. Richter and O.M. Lovera are supported by National Science Foundation grant NSF-EAR 87-07520. O.M. Lovera also thanks the Consejo Nacional de Investigaciones Cientificas y Técnicas de la República de Argentina for additional financial support. T.M. Harrison and P. Copeland are also supported by the Department of Energy and the National Science Foundation, including NSF grant EAR 87-21026.

References

1 O.M. Lovera, F.M. Richter and T.M. Harrison, $^{40}Ar/^{39}Ar$ thermochronometry for slowly cooled samples having a distribution of diffusion domain sizes, J. Geophys. Res. 94, 17,917–17,935, 1989.

2 G. Tu, Y. Zhang, Z. Zhao and Z. Wang, Characteristics and evolution of granitoids of southern Xizang, in: Proc. of Symposium on Qinghai-Xizang (Tibet) Plateau, Vol. 1. Geology, Geological History and Origin of Qinghai Xizang Plateau, pp. 353–361, 1981.

3 F. Debon, P. Le Fort, S.M.F. Sheppard and J. Sonet, The four plutonic belts of the Transhimalaya-Himalaya: a chemical, mineralogical, isotopic, and chronological synthesis along a Tibet-Nepal section, J. Petrol. 21, 219–250, 1986.

4 U. Schärer, R.-H. Xu and C.J. Allègre, U-Pb geochronology of the Gangdese (Transhimalaya) plutonism in the Lhasa-Xigase region, Tibet, Earth Planet. Sci. Lett. 69, 311–320, 1984.

5 R.-H. Xu, U. Schärer and C.J. Allègre, Magmatism and metamorphism of the Lhasa block (Tibet): a geochronological study, J. Geol. 93, 41–57, 1985.

6 J. Besse, V. Courtillot, J.P. Pozzi, M. Westphal and Y.X. Zhou, Paleomagnetic estimates of crustal shortening in the Himalayan thrusts and Zangbo suture, Nature 311, 621–626, 1984.

7 P. Patriat and J. Achache, India-Eurasia collision chronology has implications for crustal shortening and driving mechanism of plates, Nature 311, 615–621, 1984.

8 P. Le Fort, The Himalayan orogenic segment, in: Tectonic evolution of the Tethyan region, A.M.C. Şengör, ed., NATO Advanced Science Institutes Series C, Kluwer, Dordrecht, 259, 289–386, 1989.

9 P. Molnar and P. Tapponnier, Cenozoic tectonics of Asia: effects of continental collision, Science 189, 419–426, 1975.

10 J.-J. Jaeger, V. Courtillot, and P. Tapponier, Paleontological view of the ages of the Deccan Traps, the Cretaceous/Tertiary boundary, and the India-Asia collision, Geology 17, 316–319, 1989.

11 J. Achache, V. Courtillot and Y.X. Zhou, Paleogeographic and tectonic evolution of southern Tibet since Middle Cretaceous time: new paleomagnetic data and synthesis, J. Geophys. Res. 89, 10,311–10,339, 1984.

12 C.T. Klootwijk, Greater India's northern extent and its underthrust of the Tibetan plateau: paleomagnetic constraints and implications, in: Zagros, Hindu Kush, Himalaya Geodynamic Evolution, H.K. Gupta and F.J. Delany, eds., Am. Geophys. Union Geodyn. Ser. 3, 313–323, 1983.

13 J.F. Dewey and K.C.A. Burke, Tibetan, Variscan and Precambrian basement reactivation: products of continental collision, J. Geol. 81, 683–692, 1973.

14 K. Burke and J.F. Dewey, Orogeny in Africa, in: African Geology, T.F. Dessavagie and A.J. Whiteman, eds., pp. 583–608, University of Ibadan Press, 1972.

15 P. Molnar and P. Tapponnier, Active tectonics of Tibet, J. Geophys. Res. 83, 5361–5375, 1978.

16 K. Burke and C. Şengör, Tectonic escape in the evolution of the continental crust, in: Reflection Seismology: The Continental Crust, Am. Geophys. Union Geodyn. Ser. 14, 41–53, 1986.

17 R. Armijo, P. Tapponnier, J.L. Mercier and Han Tong-Lin, Quaternary extension in southern Tibet: field observations and tectonic implications, J. Geophys. Res. 91, 13,803–13,872, 1986.

18 I. McDougall and T.M. Harrison, Geochronology and thermochronology by the $^{40}Ar/^{39}Ar$ method, in: Oxford Monographs on Geology and Geophysics, 9, 212 pp. Oxford Univ. Press, Oxford, 1988.

19 M.H. Dodson, Closure temperature in cooling geochronological and petrological systems, Contrib. Mineral. Petrol. 40, 259–274, 1973.

20 O.M. Lovera, F.M. Richter and T.M. Harrison, Diffusion domains determined by ^{39}Ar released during step heating, J. Geophys. Res. (in press).

21 T.M. Harrison, O.M. Lovera and M.T. Heizler, $^{40}Ar/^{39}Ar$ results for alkali feldspars containing diffusion domains with differing activation energy, Geochim. Cosmochim. Acta (in press).

22 P. Copeland, T.M. Harrison, W.S.F. Kidd, X. Ronghua and Z. Yuquan, Rapid early Miocene acceleration of uplift in the Gangdese Belt, Xizang (southern Tibet), and its bearing on the accommodation mechanism of the India-Asia collision, Earth Planet. Sci. Lett. 86, 240–252, 1987.

23 T.M. Harrison and J.D. FitzGerald, Exsolution in hornblende and its consequences for $^{40}Ar/^{39}Ar$ age spectra and closure temperature, Geochim. Cosmochim. Acta 50, 247–274, 1986.

24 P. Copeland, Cenozoic tectonic history of the southern Tibet Plateau and the eastern Himalaya: Evidence from $^{40}Ar/^{39}Ar$ dating, Ph.D. dissertation, State Univ. of New York at Albany, 414 pp., 1990.

25 M.C. Johnson and M. Rutherford, Experimental calibration of the aluminium-in-hornblende geobarometer with application to Long Valley caldera (California) volcanic rocks, Geology 17, 837–841, 1989.

26 T.M. Harrison and G.K.C. Clarke, A model of the thermal effects of igneous intrusion and uplift as applied to the Quottoon Pluton, British Columbia, Can. J. Earth Sci. 16, 411–420, 1979.

27 J.G. Sclater, B. Parsons and C. Jaupart, Oceans and continents: similarities and differences in the mechanisms of heat loss, J. Geophys. Res. 86, 11,535–11,552, 1981.

28 F.M. Richter, Dynamical models for sea floor spreading, Rev. Geophys. Space Phys. 11, 223–287, 1973.

29 J. Yu and F. Yu, The altitude and latitude effects of H-O isotopic systems in granitoid rocks, Sci. Sin. (Ser. B) XXXI, 748–759, 1988.

30 W.S.F. Kidd, Y. Pan, C. Chang, M.P. Coward, J.F. Dewey, A. Gansser, P. Molnar, R.M. Shackleton and Y. Sun, Geological mapping of the 1985 Chinese-British Tibetan (Xizang-Qinghai) Plateau Geotraverse route, Philos. Trans. R. Soc. London A Ser. 327, 287–305, 1988.

31 T.M. Harrison and I. McDougall, The thermal significance of potassium feldspar K-Ar ages infered from $^{40}Ar/^{39}Ar$ age spectrum results, Geochim. Cosmochim. Acta 46, 1811–1820, 1982.